

## New Aspects of the Mixed State from Six-Terminal Measurements on $\text{Bi}_2\text{Sr}_2\text{CaCu}_2\text{O}_x$ Single Crystals

R. Busch,<sup>(1),(2)</sup> G. Ries,<sup>(2)</sup> H. Werthner,<sup>(1)</sup> G. Kreiselmeyer,<sup>(1)</sup> and G. Saemann-Ischenko<sup>(1)</sup>

<sup>(1)</sup>Physikalisches Institut, Universität Erlangen-Nürnberg, Erwin-Rommel-Strasse 1, W-8520 Erlangen, Federal Republic of Germany

<sup>(2)</sup>Siemens AG, Research Laboratories, Postfach 3220, W-8520 Erlangen, Federal Republic of Germany

(Received 29 January 1992; revised manuscript received 10 April 1992)

We attached two current and two voltage contacts on both sides of  $\text{Bi}_2\text{Sr}_2\text{CaCu}_2\text{O}_x$  single crystals and performed transport measurements applying the current parallel to the  $\text{CuO}_2$  layers. In the Ohmic regime, the voltage signal on the side of the current contacts was more than a factor of 100 larger than at the opposite side. The results are interpreted within an anisotropic resistivity model to obtain the true resistivities  $\rho_{ab}(B, T)$  and  $\rho_c(B, T)$ . A model is presented based on the movement of pancake vortices involving vortex shear, vortex cutting, and generation of Josephson vortices between the layers.

PACS numbers: 74.60.Ge, 72.15.Eb

Recent developments in the theory of the mixed state of high- $T_c$  superconductors focus on the layered structure of these materials. According to [1-4] a vortex is a stack of two-dimensional point vortices which are confined to the  $\text{CuO}_2$  planes. The electric transport properties of these materials have been explained by the evaporation [4] or a 3D-2D transition of these vortex stacks [5,6]. Melting [7], entanglement [8], or a vortex liquid-glass transition [9] of the vortex lattice were proposed as well. As a more conventional mechanism thermally activated depinning of vortices was proposed [4,10-13].

In order to gain more information about the dynamical state of the vortex lattice in the resistive regime of these materials we performed six-terminal-transport measurements on two  $\text{Bi}_2\text{Sr}_2\text{CaCu}_2\text{O}_x$  single crystals in the mixed state. The aim of our work was to discriminate whether the vortices in the superconductor move as three-dimensional entities in the form of flux tubes or incoherently as two-dimensional objects within the  $\text{CuO}_2$  planes. The inset in Fig. 1 shows schematically the arrangement with two current and two voltage contacts attached at both wide sides of the crystal. The field was applied perpendicularly to the  $\text{CuO}_2$  planes.

Applying the current only on one side inevitably implies a current component perpendicular to the  $\text{CuO}_2$  planes. This may possibly generate an electric field component normal to the basal plane and consequently an inhomogeneous current distribution inside the sample. To test this we also recorded the voltage signal  $V_{\text{bot}}$  on the crystal face opposite to the current contacts.

We used two single crystals grown from the melt using  $\text{Al}_2\text{O}_3$  crucibles [14]. The size of the crystals was about  $4.2 \times 1.5 \times 0.014 \text{ mm}^3$  and  $2.6 \times 1.3 \times 0.011 \text{ mm}^3$ , hereafter referred to as crystals 1 and 2, respectively. Their critical temperatures were 87 and 88 K with transition widths of  $\Delta T = 3$  and 6 K at zero field. The current and voltage contacts are sputtered silver dots with diameters of 0.4-0.6 and 0.3-0.4 mm, respectively, and were attached with silver plummet on silver layers sputtered through a mask. After tempering the contacts had resistivities less

than  $1 \Omega$  at room temperature [15]. The distances between the current contacts were 2.5 and 1.9 mm for samples 1 and 2, respectively; those between the voltage contacts were 1.2 and 0.7 mm.

In the field region of 0.01 to 2 T and for temperatures  $T \gtrsim 35 \text{ K}$  we recorded voltage-current curves  $V_{\text{top}}(I)$  and  $V_{\text{bot}}(I)$  for different temperatures. The current was varied from  $10^{-6}$  to  $10^{-1} \text{ A}$ . In general voltage-current relations were linear up to 20-50 mA and showed positive curvature above probably due to thermal effects [11]. At low temperatures and low fields we found nonlinear be-

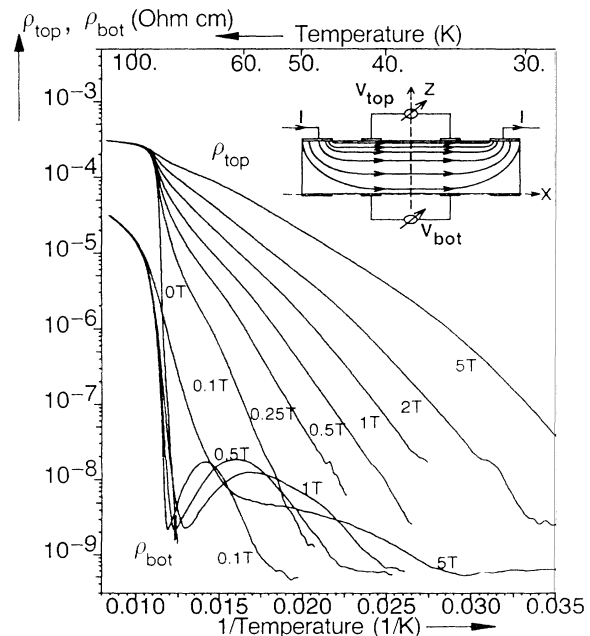


FIG. 1. Nominal resistivities  $\rho_{\text{top}}$  and  $\rho_{\text{bot}}$  calculated from  $V_{\text{top}}$  and  $V_{\text{bot}}$ , respectively, assuming uniform distributed current density within the crystal for an applied current of 10 mA. For reasons of clarity we omitted  $\rho_{\text{bot}}$  for 0, 0.25, and 2 T. Inset: Schematic picture of the attachment of the contacts on the single crystals and the current-voltage configuration.

havior  $V_{\text{top}} \propto I\rho$ , and the voltage  $V_{\text{bot}}$  was below the resolution of our nanovoltmeter. Only the regime of Ohmic behavior was included into our further analysis. Figure 1 shows effective electrical resistivities of crystal 1 as obtained from the top and bottom voltage signals anticipating uniform current density within the sample volume. The current was  $I=10$  mA. In this representation the curves  $\rho_{\text{top}}$  follow the typical Arrhenius behavior  $\ln\rho \propto -U_0/T$  as is usually observed on single crystals [11] and films [5]. Our values for  $\rho_{\text{top}}$  agree well with  $\rho(B, T)$  obtained by Palstra *et al.* [12] on a similar crystal. The important point to note is the large difference of a factor of  $10^2$ – $10^4$  in the voltages recorded on both sides of the 14- $\mu\text{m}$ -thick crystal. This implies an appreciable voltage drop along the  $c$  axes and indicates that also the current distribution within the crystal is nonuniform. The  $\rho_{\text{bot}}$  curves show a strange nonmonotonic behavior which we will comment on later. Crystal 2 showed qualitatively the same behavior.

Exchanging the current and voltage contacts from top to bottom gave the same behavior with a difference of a factor of 2.5 in the absolute value. It may probably be explained by differences in the surfaces of the sample.

It is evident that the "true" resistivities  $\rho_{ab}$  and  $\rho_c$  parallel and perpendicular to the  $a$ - $b$  plane cannot be obtained directly from the measured voltage and current. To take account of the nonuniform current distribution we proceed with the development of a linear anisotropic resistivity model. For the two-dimensional potential distribution  $V(x, z)$  the following differential equation has to be solved:

$$\text{div} j = \frac{1}{\rho_{ab}} \frac{d^2 V}{dx^2} + \frac{1}{\rho_c} \frac{d^2 V}{dz^2} = 0. \quad (1)$$

An appropriate solution is given by an expansion

$$V(x, z) = \sum_{n=1,3,5,\dots} V_n \sin\left[\frac{n\pi x}{L}\right] \cosh\left[\left(\frac{\rho_c}{\rho_{ab}}\right)^{1/2} \frac{n\pi z}{L}\right]. \quad (2)$$

$L$  denotes the length of the sample; the  $a$ - $b$  and  $c$  axis correspond to the  $x$  and  $z$  coordinates of the coordinate system included in Fig. 1. Each component satisfies the surface boundary condition of the vanishing normal field component at the bottom of the sample at  $z=0$  and at the edges at  $x = \pm L/2$ . The coefficients  $V_n$  have to be chosen such that on the top surface  $z=D$  ( $D$  denotes the thickness of the sample) the normal component  $j_n = -\rho_c^{-1} dV/dz$  just represents the current injection beneath the current contact pads and zero in between. From Eq. (2) it follows that the short-wavelength components decay effectively with the distance from the current contacts. In the volume of the sample we may approximate  $V(x, z)$  by the lowest  $n=1$  term alone. From the condition that the applied current  $I$  must equal the integrated current density  $I = b \int_0^D j_x dz$ , e.g., in the

midplane  $x=0$  of the crystal, the coefficient  $V_1$  is then uniquely determined and one obtains

$$V(x, z) \approx -\frac{I}{b} (\rho_c \rho_{ab})^{1/2} \frac{\sin(\pi x/L)}{\sinh[(\pi D/L)(\rho_c/\rho_{ab})^{1/2}]} \times \cosh\left[\frac{\pi z}{L} \left(\frac{\rho_c}{\rho_{ab}}\right)^{1/2}\right]. \quad (3)$$

$b$  is the width of the sample in the  $y$  direction.

Identifying now Eq. (3) at positions  $(x_i, z_i)$  of the voltage tabs with the recorded voltages  $V_{\text{top}}$  and  $V_{\text{bot}}$  we may then resolve this equation.

From the ratio  $V_{\text{top}}/V_{\text{bot}}$  we obtain

$$\left(\frac{\rho_c}{\rho_{ab}}\right)^{1/2} \approx \frac{L}{\pi D} \text{arccosh}(V_{\text{top}}/V_{\text{bot}}) \quad (4)$$

and further from  $V_{\text{top}}$

$$(\rho_c \rho_{ab})^{1/2} \approx \frac{V_{\text{top}} b}{2I \sin[\pi(x_2 - x_1)/2L]} \times \tanh\left[\frac{\pi D}{L} \left(\frac{\rho_c}{\rho_{ab}}\right)^{1/2}\right]. \quad (5)$$

$x_1$  and  $x_2$  denote the coordinates of the voltage contacts.

We compared Eqs. (4) and (5) with those obtained

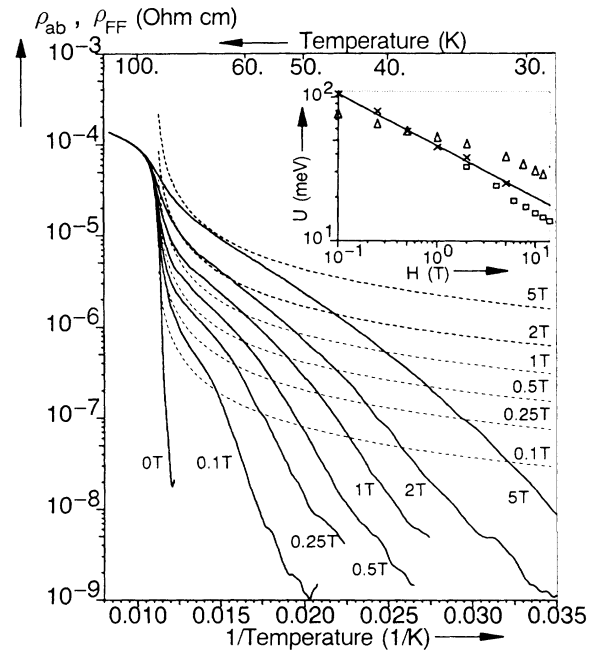


FIG. 2. Resistivities in the  $a$ - $b$  plane of the crystal determined from the measured data by Eqs. (4) and (5) (solid lines) and by the Bardeen-Stephen model (dashed lines). Inset: Pinning energies determined by the slope of the low-temperature tail of the resistivity curves in the  $a$ - $b$  plane plotted against the applied magnetic field.  $\Delta$ , Palstra *et al.* [11] data;  $\square$ , Kobayashi *et al.* [20] data;  $\times$ , our data; the straight line indicates the  $H^{-0.36}$  law.

with a different method by Montgomery [16] and Logan, Rice, and Wick [17]. Within the appropriate approximations we found agreement for  $(\rho_c/\rho_{ab})^{1/2}$  and a discrepancy of a factor of  $\pi/4$  for  $(\rho_c\rho_{ab})^{1/2}$ . This factor appears in Eq. (11) of [17] with no comment about its origin.

Equations (4) and (5) have been resolved further to give the true resistivities  $\rho_{ab}$  and  $\rho_c$  for crystal 1 which are shown in Figs. 2 and 3. The results for crystal 2 are similar. If we approximate in Eq. (5) the tanh for large arguments and linearize the sin we obtain  $(\rho_c\rho_{ab})^{1/2} \approx (V_{top}bL)/I\pi(x_2 - x_1)$ , whereas the standard treatment [12] would give  $\rho_{ab} = (V_{top}bD)/I(x_2 - x_1)$ . The effect of nonuniform current distribution is that  $V_{top}$  measures  $(\rho_{ab}\rho_c)^{1/2}$  and not  $\rho_{ab}$  alone. Furthermore, we see that the thickness  $D$  of the sample is replaced by the length  $L/\pi$  which reflects the fact that the current does not occupy the whole cross section. Using Eq. (3) and  $j_x = -\rho_{ab}^{-1}dV/dx$  we can derive an expression for the current density within the sample. One important result of our experiment is that the current penetrates exponentially damped into the crystal and is confined to a thin surface layer of thickness  $z_{eff}$ :

$$j_x(z) \approx j_x^0 \exp(-|z|/z_{eff}), \tag{6}$$

where  $z_{eff} = L\pi^{-1}(\rho_{ab}/\rho_c)^{1/2} \approx 1-2 \mu\text{m}$  in our case. Only in thin films is the cross section fully utilized. This may be a possible reason, among others, for the high current-carrying capacity of thin films as compared to bulk material.

Usually transport measurements on superconductors are interpreted on the basis of the Anderson-Kim flux

creep theory [18], which in its linearized form [19] gives

$$\rho_{TAFF} = E/J = \rho_0 \exp(-U/k_B T). \tag{7}$$

$\rho_{TAFF}$  is the so-called thermally assisted flux flow resistivity and describes the observed Arrhenius behavior of  $\rho_{ab}$ . We determined the pinning energies  $U$  from the slope of the low-temperature tail of the curves in Fig. 2. In the inset we plotted  $U(B)$  together with those obtained by Palstra *et al.* [11] and Kobayashi *et al.* [20]. Whereas Palstra *et al.* found pinning energies which scale as  $H^{-1/6}$  for fields lower than 1 T our data can be fitted by  $U \propto H^{-0.36}$ .

In the regime of high flux creep rates beyond  $10^{-6} \Omega\text{cm}$   $\rho_{ab}$  deviates from the Arrhenius behavior. We argue that here the viscous damping of moving vortices cannot be neglected [12]. In Fig. 2 we demonstrate that  $\rho_{ab}$  indeed approaches the dashed lines representing the flux flow resistivity  $\rho_{FF}$ . It is calculated with the Bardeen-Stephen (BS) model  $\rho_{FF} = \rho_n(T)B/B_{c2}(T)$  [21] using a linear extrapolation of  $\rho_n(T)$  below  $T_c$  and  $dB_{c2}/dT = -1.8 \text{ T/K}$ .

Even though the BS model does not account for the layered structure of high- $T_c$  superconductors there is fairly good agreement with the measured data for  $T > 60 \text{ K}$ . In this regime the viscous drag force rather than thermal activation determines the flux dynamics.

In some measurements we used two opposing current contacts on the top and bottom sides applying the current along the  $c$  axis of the crystal. We found linear  $V$ - $I$  relations in the same temperature and field region as for the previous measurement. In Fig. 3 we compare the resistivities in the  $c$  direction calculated from  $V_{top}$  and  $V_{bot}$  using Eqs. (4) and (5) (solid lines) with those obtained by measurements where the current was applied between two opposing current contacts perpendicular to the  $\text{CuO}_2$  planes (dashed lines), using the standard formula  $\rho_c = (V/D)/(I/bL)$ . The deviations between the two results can be related to the neglected voltage drop in the  $a$ - $b$  direction and the nonuniform current distribution.  $\rho_c$  also follows an Arrhenius law. The knee close to  $T_c$  gives rise to a minimum in the effective penetration depth  $z_{eff}$  in Eq. (6) and is the reason for the dip in  $\rho_{bot}$  in Fig. 1.

Beyond the scope of the anisotropic resistivity model our results have implications for the dynamic nature of the vortex lattice in the mixed state. As long as phase coherence within the layers is maintained, the voltage in a superconductor implies movement of vortices with a transverse velocity  $v_y$ :  $E_x = v_y B_z$ . Then according to our results  $V_{top} \gg V_{bot}$  the vortices on the side of current contacts must run accordingly faster than on the opposite side. If we regard vortices as continuous objects passing through the crystal this essentially means longitudinal shear with a shear angle and a transverse component of the associated magnetic flux which grows infinitely with time. To resolve this obvious contradiction there must be a relaxation mechanism which reduces this vortex shear

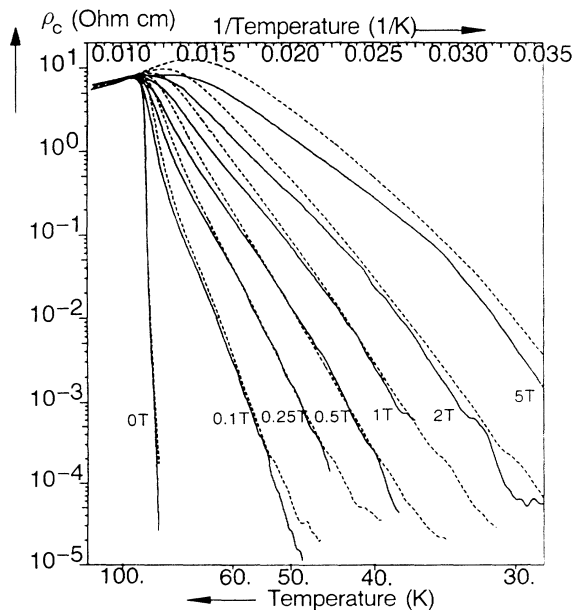


FIG. 3. Resistivity perpendicular to the  $a$ - $b$  plane of the crystal determined from the measured data by Eqs. (4) and (5) (solid lines) and by standard evaluation (dashed lines).

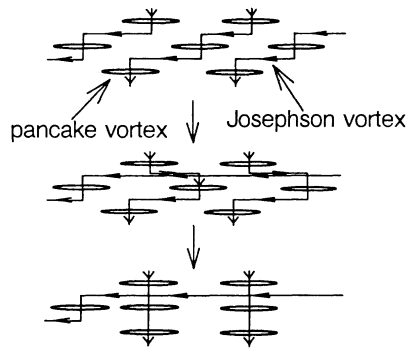


FIG. 4. Generation of Josephson vortices and shear relief in a tilted pancake vortex lattice. Ellipses denote pancake vortices in the  $\text{CuO}_2$  layers.

to obtain a dynamic steady state of flux movement and in the same turn allows for potential differences between adjacent  $\text{CuO}_2$  double layers. We suppose that this is provided by Josephson vortices which are located between the layers [22]. To explain the origin of these Josephson vortices and their role for reducing the vortex shear we propose a mechanism, based on the Lawrence-Doniach model [1], which is shown in Fig. 4. Upon increasing shear the Josephson vortices are continuously elongated and may recombine to form longer segments by losing the connection to the pancake vortices. This represents a volume source of independent Josephson vortices. Driven by the normal component  $j_z$  these move to the edges of the sample providing a continuous phase slip and thus a voltage difference between the  $\text{CuO}_2$  layers. The pancake vortices in adjacent layers in turn lose their prior connection via the interplanar vortex pieces and rearrange newly to form an energetically favorable configuration with less shear.

In summary, we determined the true resistivities  $\rho_{ab}$  and  $\rho_c$  for  $\text{Bi}_2\text{Sr}_2\text{CaCu}_2\text{O}_x$  single crystals using samples with two current and two voltage contacts on each surface. We found that the ratio of  $\rho_{ab}$  and  $\rho_c$  is about  $10^5$  and that  $\rho_{ab}$  is related to both flux flow and to the linearized flux creep resistivity. The current density is mainly restricted to a layer of  $1-2 \mu\text{m}$  on the side of the current contacts. We concluded furthermore that the vortices must be kinked due to the nonuniform current distribution in the crystal and proposed a model which explains shear relief and generation of Josephson vortices in the vortex lattice. We expect that also at lower temperatures in the regime of non-Ohmic behavior the above conclusions remain qualitatively correct. In particular the existence of a finite penetration depth of the transport current into the sample implies that one regard values for critical current densities with caution.

We thank W. Gerhäuser for preparing the single crystals and H. W. Neumüller for the permission to use the facilities at the Siemens laboratories in order to prepare the samples and to perform premeasurements. This work was supported by the Bundesministerium für Forschung und Technologie.

- 
- [1] W. E. Lawrence and S. Doniach, in *Proceedings of the Twelfth International Conference on Low Temperature Physics, Kyoto, 1970*, edited by E. Kanda (Keigaku, Tokyo, 1971), p. 361.
  - [2] L. N. Bulaevskii, *Zh. Eksp. Teor. Fiz.* **64**, 2241 (1973) [*Sov. Phys. JETP* **37**, 1133 (1973)].
  - [3] K. B. Eftov, *Zh. Eksp. Teor. Fiz.* **76**, 1781 (1979) [*Sov. Phys. JETP* **49**, 905 (1979)].
  - [4] J. R. Clem, *Phys. Rev. B* **43**, 7837 (1991).
  - [5] D. H. Kim, K. E. Gray, R. T. Kampwirth, and D. M. McKay, *Phys. Rev. B* **42**, 6249 (1990).
  - [6] P. Schmitt, P. Kummeth, L. Schultz, and G. Saemann-Ischenko, *Phys. Rev. Lett.* **67**, 267 (1991).
  - [7] P. L. Gammel, L. F. Schneemeyer, J. V. Waszczak, and D. J. Bishop, *Phys. Rev. Lett.* **61**, 1666 (1988).
  - [8] D. R. Nelson, *Phys. Rev. Lett.* **60**, 1973 (1988).
  - [9] R. H. Koch, V. Foglietti, W. J. Gallagher, G. Koren, A. Gupta, and M. P. A. Fisher, *Phys. Rev. Lett.* **63**, 1511 (1989).
  - [10] A. Gupta, P. Esquinazi, H. F. Braun, and H. W. Neumüller, *Phys. Rev. Lett.* **63**, 1869 (1989).
  - [11] T. T. M. Palstra, B. Batlogg, L. F. Schneemeyer, and J. V. Waszczak, *Phys. Rev. Lett.* **61**, 1662 (1988).
  - [12] T. T. M. Palstra, B. Batlogg, R. B. van Dover, L. F. Schneemeyer, and J. V. Waszczak, *Phys. Rev. B* **41**, 6621 (1990).
  - [13] W. Gerhäuser, G. Ries, H. W. Neumüller, W. Schmidt, O. Eibl, G. Saemann-Ischenko, and S. Klaumünzer, *Phys. Rev. Lett.* **68**, 879 (1992).
  - [14] W. Gerhäuser, H. W. Neumüller, W. Schmidt, G. Ries, G. Saemann-Ischenko, H. Gerstenberg, and F. M. Sauerzopf, *Physica (Amsterdam)* **185-189C**, 2273 (1991).
  - [15] H. Werthner, diploma thesis, Erlangen, 1992 (unpublished).
  - [16] H. C. Montgomery, *J. Appl. Phys.* **42**, 2971 (1971).
  - [17] B. F. Logan, S. O. Rice, and R. F. Wick, *J. Appl. Phys.* **42**, 2975 (1971).
  - [18] P. W. Anderson and Y. B. Kim, *Rev. Mod. Phys.* **36**, 39 (1964).
  - [19] E. H. Brandt, *Physica (Amsterdam)* **169B**, 91 (1991).
  - [20] N. Kobayashi, H. Iwasaki, H. Kawabe, K. Watanabe, H. Yamane, H. Kurosawa, H. Masumoto, T. Hirai, and Y. Muto, *Physica (Amsterdam)* **159C**, 295 (1989).
  - [21] J. Bardeen and M. J. Stephen, *Phys. Rev.* **140**, A1197 (1965).
  - [22] R. Kleiner, F. Steinmeyer, G. Kunkel, and P. Müller, *Phys. Rev. Lett.* **68**, 2394 (1992).